magnetochemistry

MDPI

Supplementary Materials: Counterintuitive Single-Molecule Magnet Behaviour in Two Polymorphs of One-Dimensional Compounds Involving Chiral BINOL-Derived Bisphosphate Ligands

Carlo Andrea Mattei, Bertrand Lefeuvre, Vincent Dorcet, Gilles Argouarch, Olivier Cador, Claudia Lalli and Fabrice Pointillart *

ISCR (Institut des Sciences Chimiques de Rennes)—UMR 6226, CNRS, Univ. Rennes, F-35042 Rennes, France; carloandrea22@libero.it (C.A.M.); bertrand.lefeuvre@univ-rennes1.fr (B.L.); vincent.dorcet@univ-rennes1.fr (V.D.); gilles.argouarch@univ-rennes1.fr (G.A.); olivier.cador@univ-rennes1.fr (O.C.); claudia.lalli@univ-rennes1.fr (C.L.)

* Correspondence: fabrice.pointillart@univ-rennes1.fr

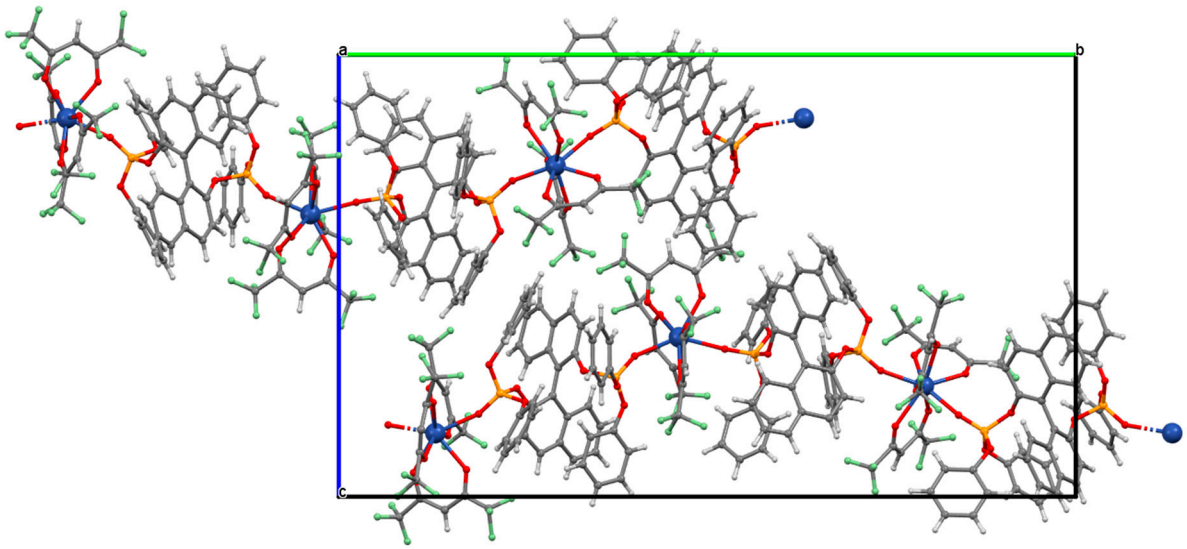

Figure S1. Fragments of two chains for the complex (*S*)-**1** (view along the axis *a*). (Dy = blue, O = red, C = dark grey, H = light grey, P = orange, F = green).

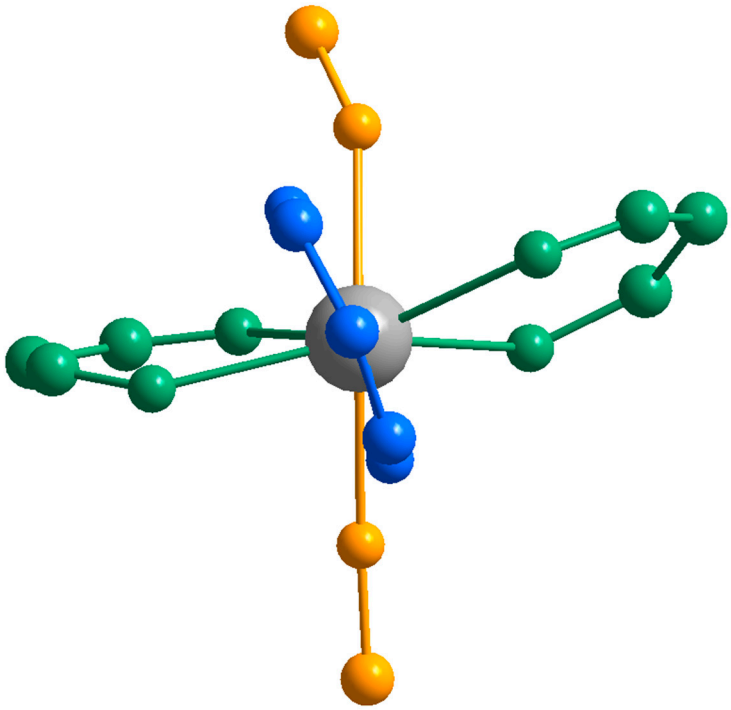

Figure S2. Representative coordination sphere of the Dy^{III} ions in both **1** and **2**. P=O, the two face-to-face $hfac^-$ and the third $hfac^-$ ligands are drawn in orange, green and blue, respectively. .

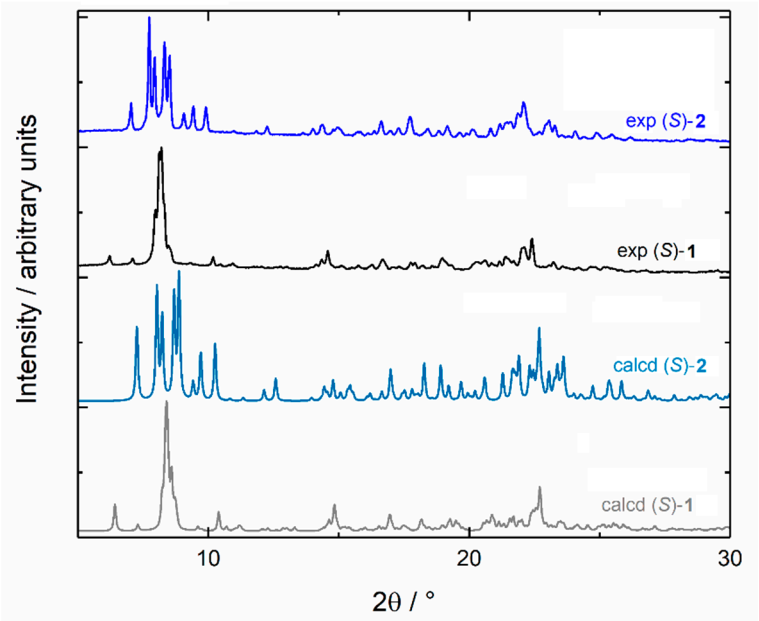

Figure S3. Superposition of experimental powder X-ray diffraction patterns from (*S*)-**2** and (*S*)-**1** measured at 300 K and simulated from (*S*)-**2** [1] and (*S*)-**1** single-crystal data obtained at 150 K.

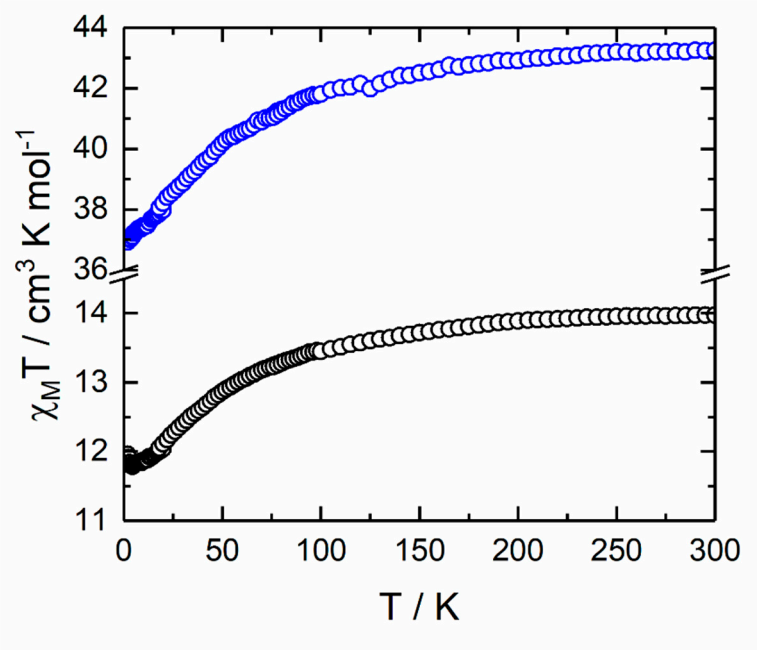

Figure S4. Temperature dependence of the $\chi_M T$ products for (*S*)-**1** (blue open circles) (given for the three crystallographically independent Dy^{III} centers) and (*S*)-**2** [1] (black open circles) in the temperature range of 2- 300 K.

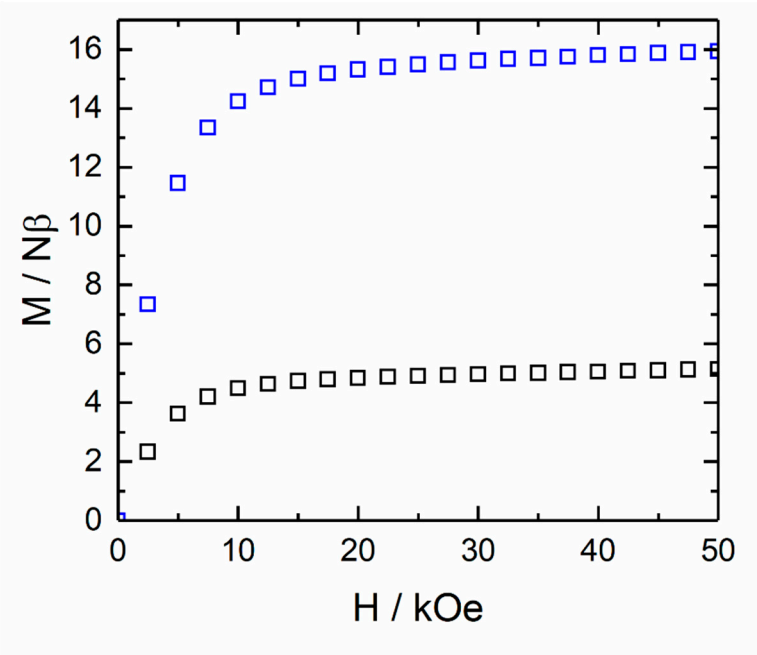

Figure S5. Field variation of the magnetization at 2 K for (*S*)-**1** (given for the three crystallographically independent Dy^{III} centers) (blue open circles) and (*S*)-**2** [1] (black open circles) in the field range of 0-5 T.

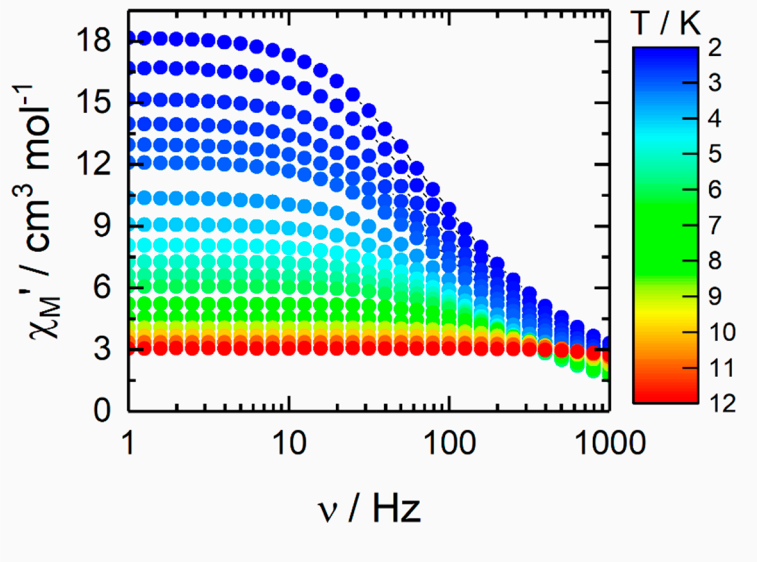

Figure S6. Frequency dependence of χ_M' zero field for (*S*)-**1** in the temperature range of 2-12 K.

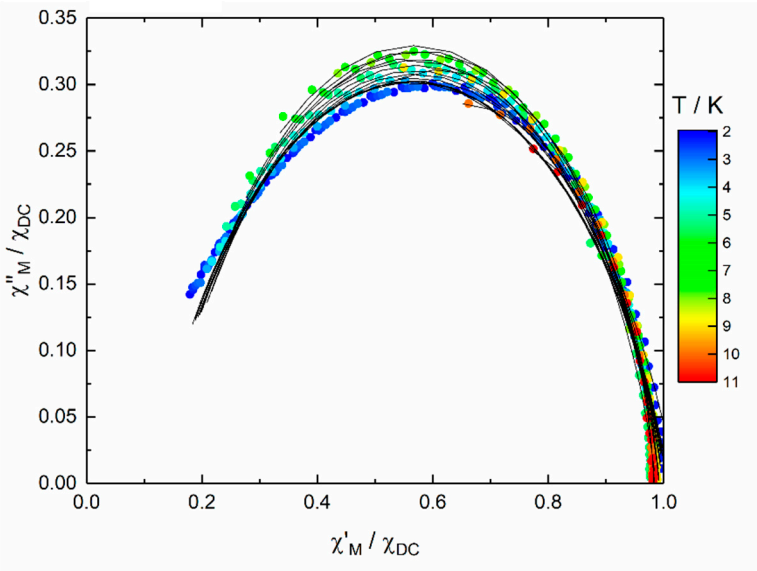

Figure S7. Normalized Argand plot of experimental (dots) and fit Debye (black lines) data for (*S*)-**1** at zero applied field in the temperature range 2-11 K.

Extended Debye model.

$$\chi_M' = \chi_S + (\chi_T - \chi_S)\frac{1+(\omega\tau)^{1-\alpha}\sin\left(\alpha\frac{\pi}{2}\right)}{1+2(\omega\tau)^{1-\alpha}\sin\left(\alpha\frac{\pi}{2}\right)+(\omega\tau)^{2-2\alpha}}$$

$$\chi_M'' = (\chi_T - \chi_S)\frac{(\omega\tau)^{1-\alpha}\cos\left(\alpha\frac{\pi}{2}\right)}{1+2(\omega\tau)^{1-\alpha}\sin\left(\alpha\frac{\pi}{2}\right)+(\omega\tau)^{2-2\alpha}}$$

With χ_T the isothermal susceptibility, χ_S the adiabatic susceptibility, τ the relaxation time and α an empiric parameter which describe the distribution of the relaxation time. For SMM with only one relaxation time, α is close to zero. The extended Debye model was applied to fit simultaneously the experimental variations of χ_M' and χ_M'' with the

frequency ν of the oscillating field ($\omega = 2\pi\nu$). Typically, only the temperatures for which a maximum on the χ_M'' vs. ν curves, have been considered. The best fitted parameters τ, α, χ_T, χ_S are listed in Tables S3-S5 with the coefficient of determination R^2.

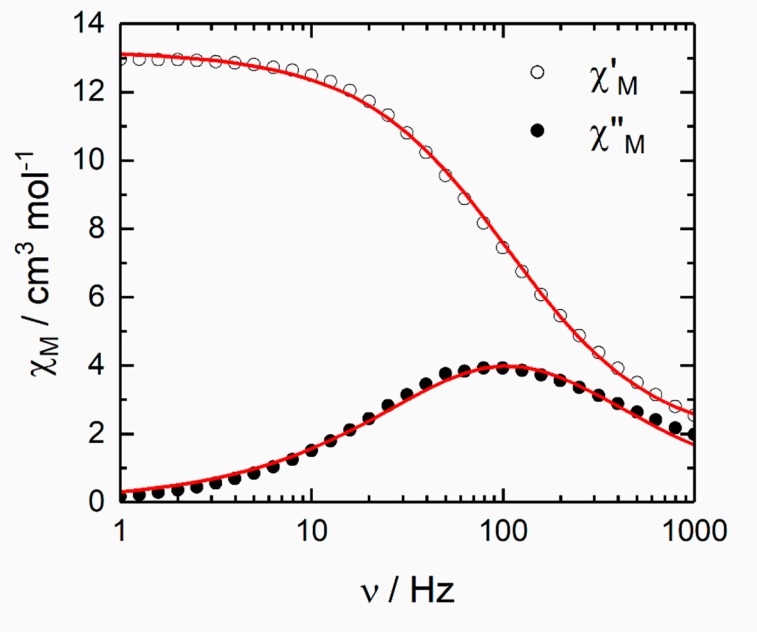

Figure S8. Frequency dependence of the in-phase (χ_M') and out-of-phase (χ_M'') components of the ac susceptibility measured on powder at 2.8 K and 0 Oe with the best fitted curves (red lines) for (*S*)-**1**.

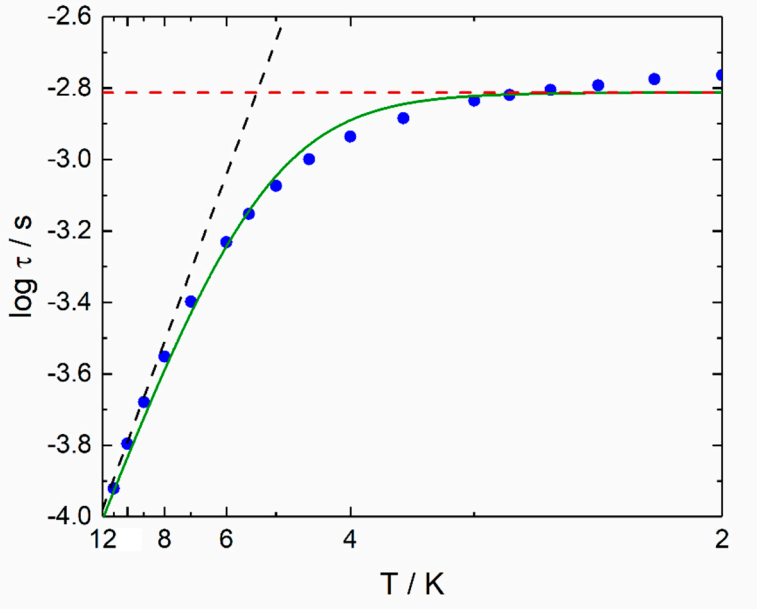

Figure S9. Temperature dependence of τ (blue spots) for (*S*)-**1** at zero applied magnetic field in the temperature range 2-11 K. The best fit curve is depicted as a full green line and the Orbach and QTM contributions are represented respectively in black dashed line and red dashed line.

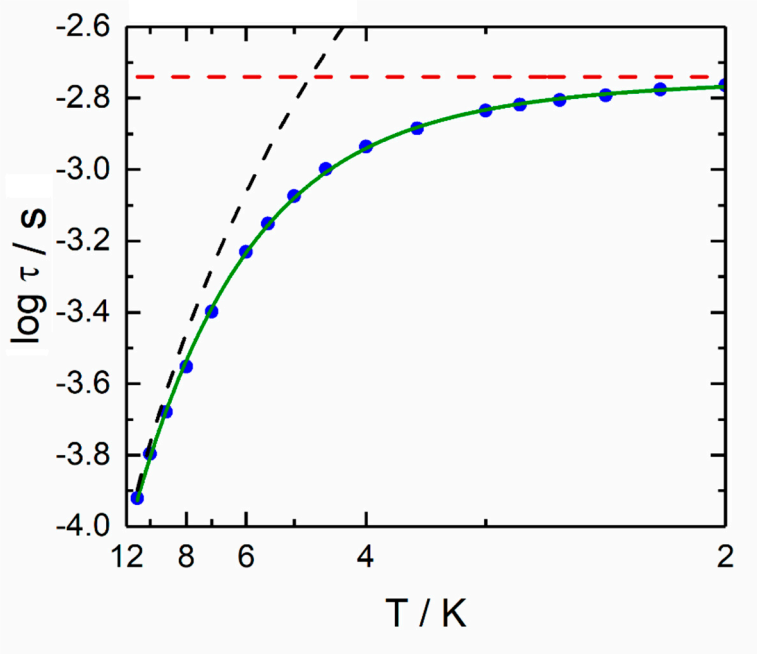

Figure S10. Temperature dependence of τ (blue spots) for (*S*)-**1** at zero applied magnetic field in the temperature range 2-11 K. The best fit curve is depicted as a full green line and the Raman and QTM contributions are represented respectively in black dashed line and red dashed line.

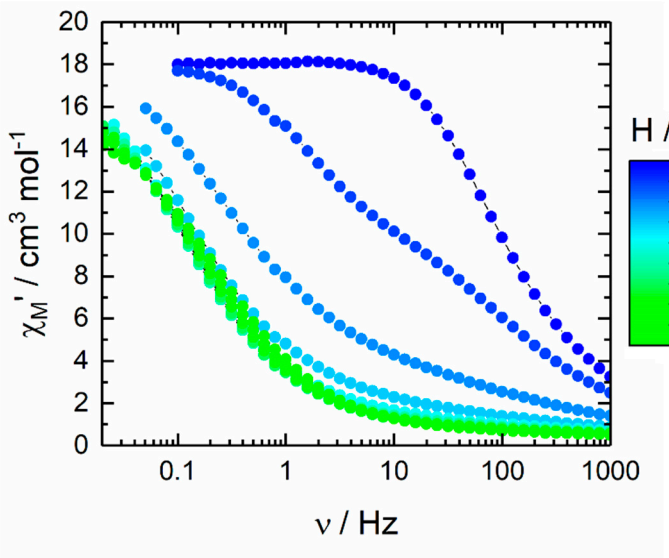

Figure S11. Frequency dependence of χ_M' for **1** at 2 K in the field range of 0-1800 Oe.

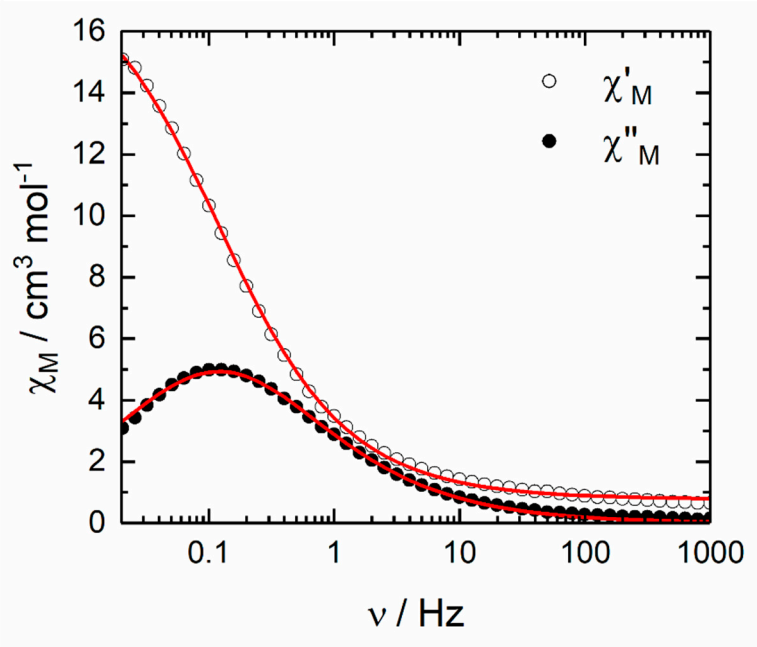

Figure S12. Frequency dependence of the in-phase (χ_M') and out-of-phase (χ_M'') components of the ac susceptibility measured on powder at 2 K and 1000 Oe with the best fitted curves (red lines) for (*S*)-**1**.

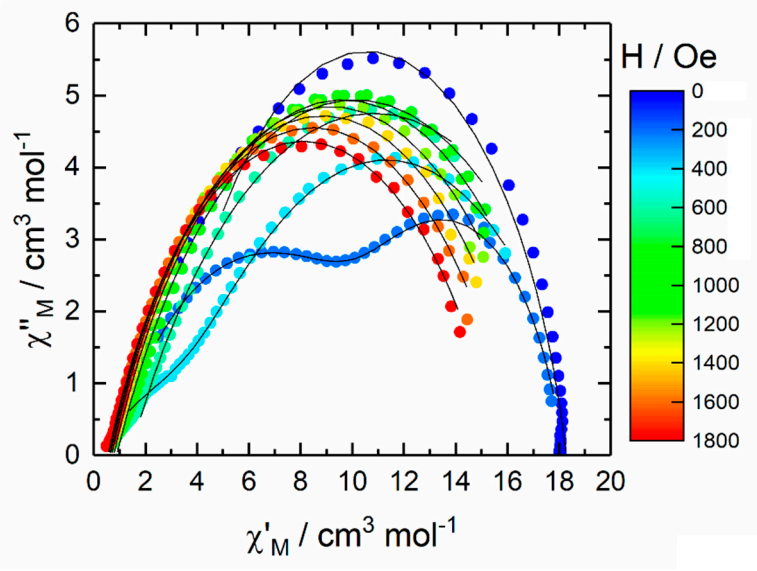

Figure S13. Argand plot of experimental (colored plots) and fit data (black lines) for **1** at 2 K in the field range 0-1800 Oe.

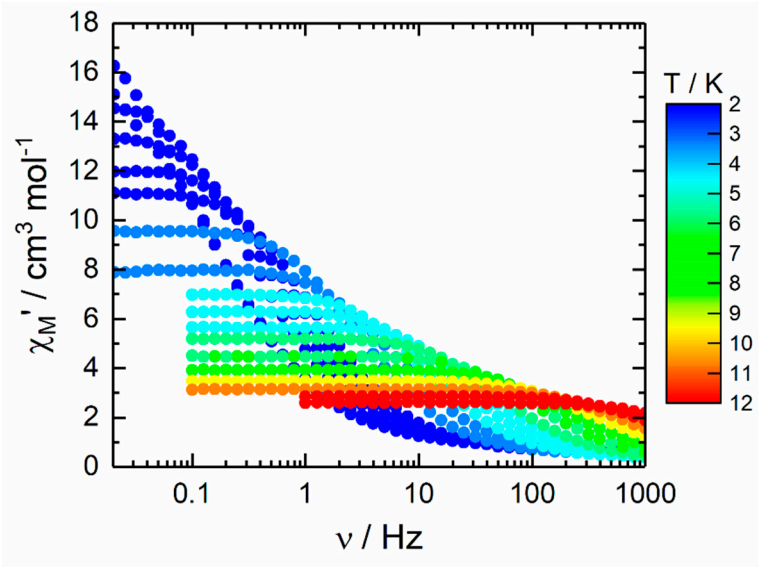

Figure S14. Frequency dependence of χ_M' under an applied magnetic field of 1000 Oe for (*S*)-**1** in the temperature range of 2-12 K.

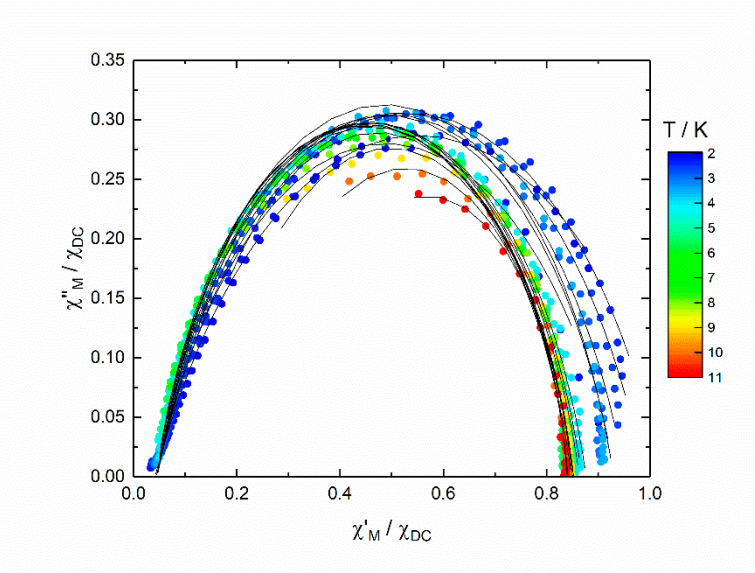

Figure S15. Normalized Argand plot of experimental (colored plots) and fit data (black lines) for **1** under an applied magnetic field of 1000 Oe in the temperature range 2-11 K.

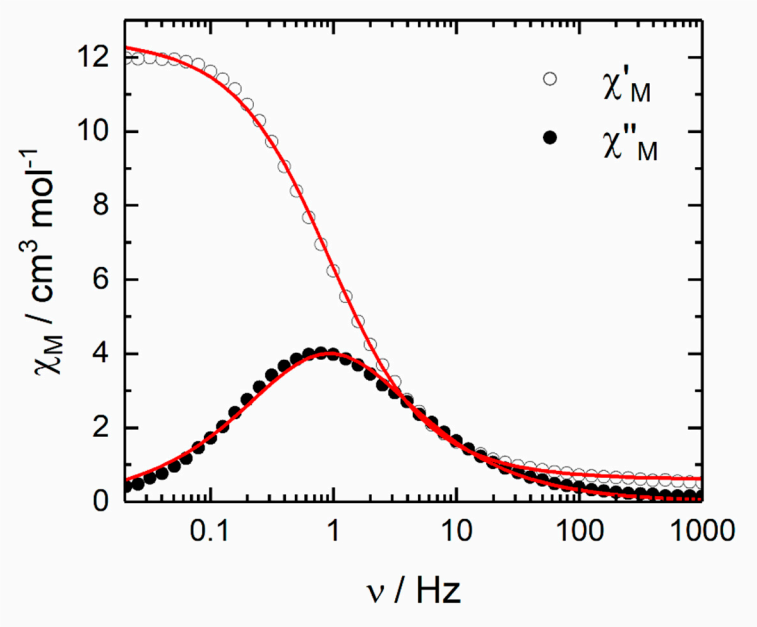

Figure S16. Frequency dependence of the in-phase (χ_M') and out-of-phase (χ_M'') components of the ac susceptibility measured on powder at 2.8 K and 1000 Oe with the best fitted curves (red lines) for (*S*)-**1**.

Table S1. X-ray crystallographic data for **1**.

Compound	**1**
Formula	$C_{177}H_{104}Dy_3F_{54}O_{42}P_6$
M / g.mol^{-1}	4601.92
Crystal system	monoclinic
Space group	P 2_1 (N° 4)
Cell parameters	a = 12.1003(12) Å b = 35.822(3) Å c = 21.466(2) Å β = 90.443(4)
Volume / Å^3	9304.1(15)
Z	2
T / K	150 K
2θ range /°	$4.24 \leq 2\theta \leq 55.164$
ρ_{calc} / g.cm^{-3}	1,643
μ / mm^{-1}	1,374
Number of reflections	88440
Independent reflections	39170
R_{int}	0.0557
$Fo^2 > 2\sigma(Fo)^2$	35776
Number of variables	1460
R_1, ωR_2	0.1362, 0.3280

Table S2. SHAPE analysis of the coordination polyhedra around the lanthanide^{III} centers in **1.**

Dy center	**CShM SAPR-8 (square antiprism D4d)**	**CShM BTPR-8 (biaugmented trigonal prism C2v)**	**CShM TDD-8 (triangular dodecahedron D2d)**	**CShM JBTPR-8 (Biaugmented trigonal prism J50)**
Dy1	0.469	1.660	2.067	1.826
Dy2	0.814	0.997	1.517	1.616
Dy3	0.657	1.490	1.772	1.905

Table S3. Best fitted parameters (χ_T, χ_S, α and τ) with the extended Debye model for compound **1** at 0 Oe in the temperature range 2-11 K.

T / K	**χ_T / cm^3 mol^{-1}**	**χ_S / cm^3 mol^{-1}**	**α**	**τ / s**	**R^2**
2	18.59610	2.09475	0.24499	1.72E-03	0.99921
2.2	17.10308	1.95451	0.24413	1.68E-03	0.99918
2.4	15.51728	1.78053	0.24244	1.61E-03	0.99920
2.6	14.28633	1.70037	0.23893	1.57E-03	0.99927
2.8	13.24476	1.61026	0.23494	1.52E-03	0.99924
3	12.34720	1.53120	0.23197	1.46E-03	0.99931
3.5	10.56555	1.38621	0.21864	1.31E-03	0.99935
4	9.23378	1.26388	0.20595	1.16E-03	0.99945
4.5	8.18765	1.16001	0.19374	1.00E-03	0.99956
5	7.36303	1.03344	0.18539	8.43E-04	0.99967
5.5	6.68510	0.95306	0.17632	7.05E-04	0.99972
6	6.12987	0.88143	0.16936	5.87E-04	0.99976
7	5.26015	0.74658	0.16182	4.00E-04	0.99978
8	4.60495	0.75950	0.15241	2.81E-04	0.99976
9	4.09330	0.96739	0.12445	2.09E-04	0.99989
10	3.68619	1.20832	0.09354	1.60E-04	0.99995
11	3.35144	1.40667	0.05627	1.20E-04	0.99994

Table S4. Best fitted parameters ($\chi_{T,1}$, χ_S, τ_1, α_1 $\chi_{T,2}$, τ_2, $\chi_{T,2}$ and α_2) with the extended Debye model for compound **1** at 2 K in the field range 0-1800 Oe.

T / K	$\chi_{T,1}$ / cm^3 mol^{-1}	χ_S / cm^3 mol^{-1}	τ_1 / s	α_1	$\chi_{T,2}$ / cm^3 mol^{-1}	α_2	τ_2 / s	R^2
0	1.83E+01	2.87E+00	1.85E-03	1.98E-01	0.00E+00	0.00E+00	1.00E+30	1.00E+00
200	7.65E+00	7.44E-01	1.13E-01	1.79E-01	1.13E+01	4.19E-01	1.61E-03	1.00E+00
400	1.42E+01	1.54E-01	6.03E-01	3.67E-01	5.03E+00	6.24E-01	2.51E-03	1.00E+00
600	2.02E+01	1.41E+00	1.29E+00	4.05E-01	—	—	—	9.99E-01
800	1.93E+01	8.92E-01	1.40E+00	3.74E-01	—	—	—	9.99E-01
1000	1.85E+01	7.75E-01	1.31E+00	3.52E-01	—	—	—	9.99E-01
1200	1.77E+01	6.98E-01	1.12E+00	3.39E-01	—	—	—	1.00E+00
1400	1.70E+01	6.41E-01	9.53E-01	3.35E-01	—	—	—	1.00E+00
1600	1.64E+01	5.94E-01	7.83E-01	3.33E-01	—	—	—	1.00E+00
1800	1.57E+01	5.53E-01	6.38E-01	3.35E-01	—	—	—	1.00E+00

Table S5. Best fitted parameters (χ_T, χ_S, α and τ) with the extended Debye model for compound **1** at 1 kOe in the temperature range 2-11 K.

T / K	χ_T / cm^3 mol^{-1}	χ_S / cm^3 mol^{-1}	α	τ / s	R^2
2	19.56908	0.76507	0.34733	1.30E+00	0.99953
2.2	15.68692	0.73605	0.28624	7.54E-01	0.99545
2.4	15.73208	0.69447	0.28913	4.42E-01	0.99941
2.6	14.03325	0.64330	0.26780	2.71E-01	0.99931
2.8	12.54221	0.59937	0.24704	1.72E-01	0.99921
3	11.46374	0.55384	0.23487	1.15E-01	0.99935
3.5	9.76356	0.48406	0.21577	4.80E-02	0.99942
4	8.09428	0.40965	0.20991	2.25E-02	0.99938
4.5	7.12262	0.35458	0.20340	1.23E-02	0.99945
5	6.39594	0.32498	0.20044	7.06E-03	0.99946
5.5	5.74641	0.31738	0.18865	4.29E-03	0.99914
6	5.26348	0.31586	0.19110	2.87E-03	0.99938
7	4.51831	0.32971	0.18457	1.37E-03	0.99946
8	3.95566	0.42122	0.17286	7.45E-04	0.99945
9	3.50686	0.59429	0.15446	4.43E-04	0.99964
10	3.15245	0.78787	0.12428	2.78E-04	0.99984
11	2.86285	1.01489	0.08767	1.79E-04	0.99992

References

1. Mattei, C.A.; Montigaud, V.; Gendron, F.; Denis-Quanquin, D.; Dorcet, V.; Giraud, N.; Riobé, F.; Argouarch, G.; Maury, O.; Le Guennic, B.; Cador, O.; Lalli, C.; Pointillart, F. Solid-state versus solution investigation of a luminescent chiral BINOL-derived bisphosphate single-molecule magnet. *Inorg. Chem. Front.* **2021**, *8*, 947-962.